ACS APPLIED MATERIALS & INTERFACES

Research Article

www.acsami.org

Space-Charge-Mediated Anomalous Ferroelectric Switching in P(VDF−TrEE) Polymer Films

Weijin Hu,[†] Zhihong Wang,[‡] Yuanmin Du,[†] Xi-Xiang Zhang,[†,‡] and Tom Wu*,[†]

[†]Physical Sciences and Engineering Division and [‡]Advanced Nanofabrication Core Lab, King Abdullah University of Science and Technology (KAUST), Thuwal 23955-6900, Saudi Arabia

Supporting Information

ABSTRACT: We report on the switching dynamics of P(VDF−TrEE) copolymer devices and the realization of additional substable ferroelectric states via modulation of the coupling between polarizations and space charges. The space-charge-limited current is revealed to be the dominant leakage mechanism in such organic ferroelectric devices, and electrostatic interactions due to space charges lead to the emergence of anomalous ferroelectric loops. The reliable control of ferroelectric switching in P(VDF−TrEE) copolymers opens doors toward engineering advanced organic memories with tailored switching characteristics.

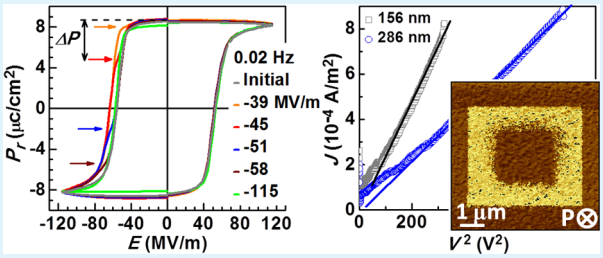

KEYWORDS: *PVDF, ferroelectric switching, defect, space charge*

I. INTRODUCTION

Reliable switching of spontaneous polarization between nonvolatile states in ferroelectric materials has enabled a flurry of electronic and data-storage technologies.[1−5] Propelled by the demands from industry, devices with higher storage density, faster writing/reading operation, and lower energy consumption have been relentlessly pursued. One generally accepted route toward higher integration densities in ferroelectric devices is to scale down the feature size of the devices, which, however, suffers from polarization instability correlated with escalated depolarization field and current leakage.[6−8] An alternative route that has attracted much attention recently is to multiply the memory states of ferroelectrics via means such as deploying ferroelectric[9] or multiferroic[10] tunneling barriers, using ferroelectric−insulator− semiconductor heterojunctions,[11] and engineering interfacial defects.[12,13] In a seminal work, Park et al. realized a tristate memory in Pt/Pb(Zr,Ti)O_3 (PZT)/Al_2O_3/ZnO/Pt capacitors by controlling the separate charge-trapping events at the PZT/Al_2O_3 and Al_2O_3/ZnO interfaces.[11] Recently, Folkman et al.[12] and Lee et al.[13] reported on the systematic manipulation of defects and their coupling with polarization in $BiFeO_3$ devices, producing multiple nonvolatile states.

It is worth noting that the above-mentioned works were all carried out on inorganic ferroelectric oxides. On the other hand, organic materials like poly(vinylidene fluoride) (PVDF) and its trifluoroethylene copolymer [P(VDF−TrEE)] can exhibit decent ferroelectric properties, and they are promising for applications such as transducers, field-effect transistors, and energy storage.[14−18] In addition, organic ferroelectrics are ideal candidates for flexible electronics, and their physical properties remain intact even after bending.[19] It is a general consensus that polarization switching in ferroelectric materials takes place through nucleation and domain growth, and defects are actively involved in this process.[20] The critical role of defects in dictating ferroelectric properties was confirmed in not only ceramic ferroelectrics[20] but also ferroelectric polymers.[21,22] Thus, it is reasonable to hypothesize that engineering switching loops can be realized in ferroelectric polymers via manipulation of the interfacial charged species, similar to reports on the inorganic counterparts. However, the electrical realization of additional nonvolatile states in PVDF polymers has not been explored so far.

In this work, we demonstrate the active control of ferroelectric switching in P(VDF−TrEE) copolymers and the electrostatically realized additional ferroelectric states in hysteresis loops. The observation of intermediate ferroelectric polarization states opens an alternative venue toward engineering the switching characteristics of organic ferroelectrics. The complementary investigation on the leakage mechanism in such capacitor devices revealed the important role of space charges in the electronic processes, and we propose the field-induced drift of space charges as the driving force in manipulating the ferroelectric loops in the P(VDF−TrEE) polymer layers.

II. EXPERIMENTAL PROCEDURE

To prepare the P(VDF-TrEE) (70/30 mol % VDF/TrFE) copolymer films, P(VDF−TrFE) powders (Piezotech S.A.) were first dissolved in diethyl carbonate, followed by passing through a poly(tetrafluoroethylene) filter with a pore size of 0.45 μm. The solution was then spin-coated onto Cu (100 nm)/Ti (10 nm)/Si(100) substrates at a speed of 3000 rpm. Subsequently, the as-coated film was

Received: July 29, 2014
Accepted: October 6, 2014
Published: October 6, 2014

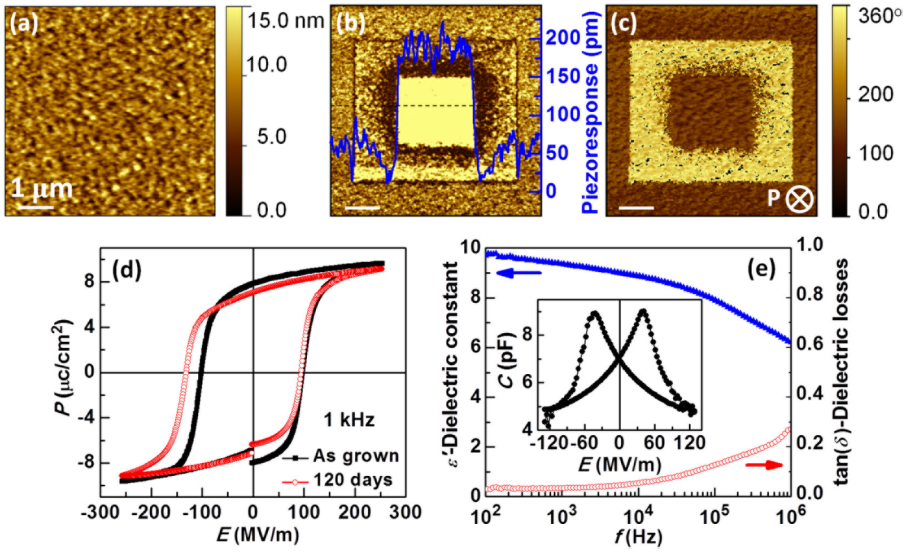

Figure 1. (a) AFM morphology image of the P(VDF−TrEE) copolymer film. (b) PFM amplitude and (c) phase images exhibiting patterned ferroelectric domains following the successive writing of two square-shaped regions with different sizes. The initial polarization is pointing down. Inset of part b: Plot of the piezoresponse profile along the dashed line. (d) Ferroelectric polarization at 1 kHz of the fresh capacitor device and that after 120 days of the device fabrication. (e) *f*-dependent dielectric constant (left) and dielectric loss (right). Inset of part e: Device capacitance as a function of the electric field.

annealed at 140 °C in air for 2 h to improve the crystallinity of the ferroelectric β phase. This annealing temperature is above the bulk paraelectric-to-ferroelectric transition temperature of ∼115 °C but below the solid-to-liquid transition temperature of ∼155 °C. The formation of a ferroelectric β phase was confirmed using an X-ray diffractometer (Bruker AXS D8 DISCOVER). The surface morphology was examined by atomic force microscopy (AFM; Veeco), and the film thickness was determined using a surface profiler (Dektak 150). The details of synthesis and characterization were given in a previous report.[23] For the ferroelectric measurements, the top copper electrodes with a size of 100 × 100 μm^2 were prepared by thermal evaporation. The polarization−electric field (*P*−*E*) loops were measured using a Radiant multiferroic tester. The quasi-static switching *I* (V) curves were collected using a Keithley 2635A multimeter. The piezoresponse force microscopy (PFM) images were measured by a commercial scanning probe microscope (MFP3D, Asylum) equipped with a lock-in amplifier. In the PFM measurements, an alternating-current voltage of 600 mV at a contact resonance frequency of ∼320 kHz was used for electrical modulation. In all of the measurements, the positive voltage corresponds to a current flowing from the top electrode to the bottom electrode, and the polarization state induced by a large positive/negative bias is defined as down/up.

III. RESULTS AND DISCUSSION

Figure 1a shows the AFM topography of a P(VDF−TrEE) film with a thickness of 66 nm. The root-mean-square roughness is 2.6 nm for a scanning area of 6 × 6 μm^2. Details on the morphology of the films with different thicknesses are provided in the Supporting Information, Figure S1. The ferroelectricity was confirmed by the out-of-plane PFM images, as shown in parts b (the amplitude image) and c (the phase image) of Figure 1. A region of 4 × 4 μm^2 was first polarized with a tip bias of −7 V, and the center region of 1.8 × 1.8 μm^2 was subsequently switched with a tip bias of 6 V. Because the phase of the as-grown film is the same as that of the center area, the initial polarization in the P(VDF−TrEE) film is down. The coarse boundary around the downward-pointing domain is also in line with the scenario that the downward polarization is more favorable. The line profile of the piezoelectric response, shown in the inset of Figure 1b, further reveals the sharp contrast of piezoresponse between the inner polarized square region and the rest of the area.

As shown in Figure 1d, the as-grown P(VDF−TrEE) film shows a well-defined *P*−*E* loop measured at 1 kHz with a remanent polarization P_r ∼ 8.2 $\mu C/cm^2$. The characteristic "butterfly" shape of the capacitance curve shown in the inset of Figure 1e further confirms the ferroelectric switching with two peaks corresponding to the reversal of polarization dipoles. Figure 1e shows the dielectric constant and dielectric loss measured over frequencies (*f*) from 100 Hz to 1 MHz. The dielectric constant is 9.8 at 100 Hz, and it decreases with increasing frequency, which is accompanied by increased dielectric loss, consistent with previous reports.[19] Overall, the ferroelectric and dielectric characteristics suggest the good quality of the device, which allows us to systematically investigate the switching behavior of the device in the quasi-static frequency region without any breakdown.

A close inspection of the *P*−*E* loop of the as-grown film in Figure 1d reveals a small negative shift of ∼1.5 MV/m in coercivity. This shift increases to ∼−18 MV/m after about 120 days. The horizontal negative shift of the *P*−*E* loop indicates that the downward polarization state is preferred relative to the upward polarization state, which is consistent with the PFM results. Such a negative imprint effect originates from the presence of an internal built-in electric field at the film−electrode interface, and the imprint effect is enhanced with time.[22,24,25] In fact, we will show that the shape of the *P*−*E* loops can be modulated by tailoring the coupling between the polarization dipoles and the accumulated charges at the interface.

The domain switching kinetics is commonly investigated by measuring the time-dependent responses of the switching current after electric pulses are applied in tailored sequences.[26] In the sequence shown in the inset of Figure 2a, the initial triangular pulse with a half-period of 65 s and a peak electric field of 115 MV/m is used to preset the sample to a full *P* state, the second square pulse with an adjustable duration time switches *P* to the opposite direction, and the amount of

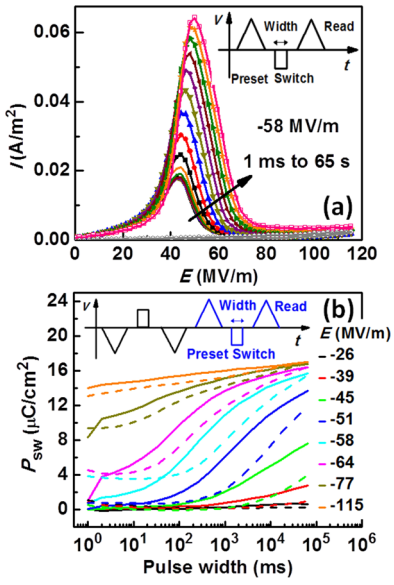

Figure 2. (a) Reading of the $I-V$ curves after square-shaped switching voltage pulses of −58 MV/m with a pulse width varying from 1 ms to 65 s. (b) Plot of the switching polarization P_{sw} versus the pulse width for various switching electric field E from −26 to −115 MV/m using both the half sequence (dashed lines) and full sequence (solid lines). The half and full sequences are illustrated in the insets of parts a and b, respectively.

switched P (P_{sw}) is read finally by the third triangular pulse with a half-period of 65 s. We named such a preset−switch−read sequence a "half sequence", and combining it with another half sequence with opposite electric polarity constitutes a full sequence (shown in the inset of Figure 2b). The main difference between the full and half sequences is that the former is symmetric with regard to the polarity of the applied electric field, whereas in the latter, extra charges are introduced into the capacitor because the switch and preset pulse processes are usually not equivalent. Thus, with the half sequence, we expect that the residual charges at the electrode−P(VDF−TrEE) interface after the switching process may couple with the ferroelectric polarization and affect the subsequent switching behavior.

Figure 2a shows the typical reading of the $I-E$ data after switching pulses with an electric field of −58 MV/m and different duration times from 1 ms to 65 s were applied. The current peak originates from the switching of the ferroelectric dipoles, which can be calculated as $P_{sw} = (1/A)(dt/dV)\int_0^V I\,dV$, where A is the area of the capacitor. With increasing width of the voltage pulse, the switching peak in the I (V) curve becomes wider and the peak current increases, suggesting that more polarizations are switched from pointing-up to pointing-down. Switching data in a full sequence (Supporting Information, Figure S2) show that the switching is easier under a positive electric field compared to the negative field case. This is consistent with the negative imprint effect observed in the $P-E$ loop and the PFM data. Figure 2b shows the plot of P_{sw} versus the duration of the switching pulse at various electric fields from −26 to −115 MV/m by using either the full (solid line) or half (dashed line) sequence. No obvious P_{sw} was observed until ∼−45 MV/m in both cases, close to the coercive field (∼56 MV/m) determined from the $P-E$ loop at 1 Hz. Interestingly, polarization switching is delayed for about a half-decade when using the half sequences compared to the full-sequence counterpart. This dependence on the previous "pulse history" is presumably correlated with the charge accumulation at the electrode−P(VDF−TrEE) interfaces in the asymmetric pulse sequences, which, in turn, couples with the ferroelectric polarizations.

The coupling between the interfacial charges and ferroelectric polarizations was further confirmed by the $I-E$ data and the corresponding $P-E$ loops. As expected, smooth $I-E$ (Figure 3a) and $P-E$ (Figure 3c) curves were collected after

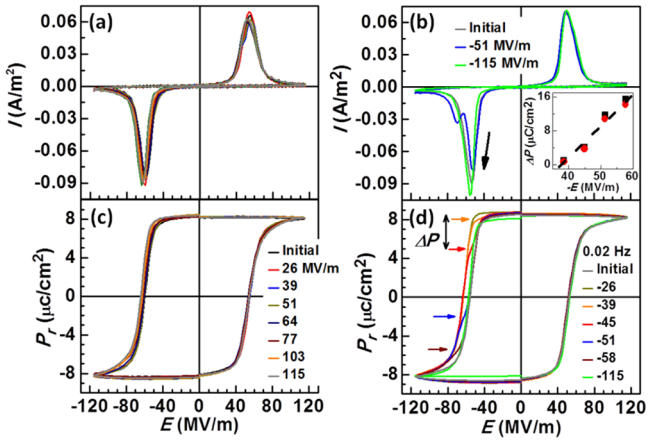

Figure 3. $I-V$ curves and the corresponding $P-E$ loops at 0.02 Hz after full-sequence (a and c) and half-sequence (b and d) measurements. Peaks and steps appear in the $I-V$ and $P-E$ loops, respectively, after the half-sequence measurements. Inset of part b: Subswitching polarization ΔP (black squares) determined from the $P-E$ loop versus the magnitudes of the switching pulse applied in the half sequence. The total switching polarizations in the half sequences (red circles, extracted from Figure 2b) are also shown for comparison. The nonswitching polarization has been calculated from the nonswitching I (V) curves and removed from the $P-E$ loops.

the full electrical pulse sequences. In contrast, after the half sequences, additional switching peaks and correspondingly subswitching steps appear in the $I-E$ (Figure 3b) and $P-E$ (Figure 3d) curves, respectively. The inset of Figure 3b shows the subswitching polarization (ΔP, black squares), determined from the $P-E$ loops with reference to the maximum polarization, as a function of the electric field applied in the switching pulse during the half-sequence measurement. Remarkably, the values of ΔP are roughly equal to the total switching polarizations during the half-sequence measurements (red circles, extracted from Figure 2b). For example, ΔP is ∼0.8 μC/cm^2 for the case of −39 MV/m and increases to ∼15 μC/cm^2 for the case of −58 MV/m. Note that the $P-E$ measurements (Figure 3d) for each electric field were carried out immediately after the half sequences (Figure 2b). This behavior indicates that the switching polarization during the half sequences will switch "normally", while the nonswitching polarization is more "stable" against the electric field, and the retarded switching gives rise to the anomalous features in the $I-E$ and $P-E$ data. Subswitching steps were also observed in the positive voltage bias after opposite pulse sequences were applied (Supporting Information, Figure S3). This flexibility makes our electrical approach different from that previously reported for metal−ferroelectric−semiconductor−metal (MFSM) devices, where additional switching peaks were observed only in one bias direction because of the asymmetry of the device structure.[27,28]

dx.doi.org/10.1021/am5050136 | ACS Appl. Mater. Interfaces 2014, 6, 19057−19063

The mechanism of modified $P-E$ loops with stable subswitching steps observed in P(VDF−TrEE) devices is rooted in the coupling between the trapped charges and polarization dipoles, similar to the inorganic counterparts.[12,13] By controlling the amplitude of the switching electric field, we could tune the positions of these substeps in a well-controlled way, as indicated by the arrows in Figure 3d and the inset of Figure 3b. From the viewpoint of applications, these substable states, in addition to the two opposite full-polarization states, provide an opportunity to realize multibit data storage in individual devices.

There are a few structure-based approaches reported in the literature toward engineering the polarization states in P(VDF−TrEE) devices. In a recent work, multibit ferroelectric P(VDF−TrEE) polymer capacitors were realized through modulation of the film thickness in a thermal imprinting process.[29] In the MFSM structures,[27,28] the semiconducting channel contributes additional capacitance and affects the polarization reversal. In this work, we took a different approach by electrically realizing the multistate switching, which is easier to implement in device fabrication and operation. Such a multilevel switching capacity could be used to enhance the data storage density of ferroelectric random access memories, where the electric ON/OFF of the semiconductor channel is controlled by the polarization state of the ferroelectric gate.[30]

Data retention and write/erase endurance are two critical parameters and are closely related to the characteristics of the polarization states. For the retention test, after different retention times from 10 to 10000 s, $P-E$ reading loops were collected after a half sequence with an electric field of −71 MV/m applied. As shown in Figure 4a, the position of the

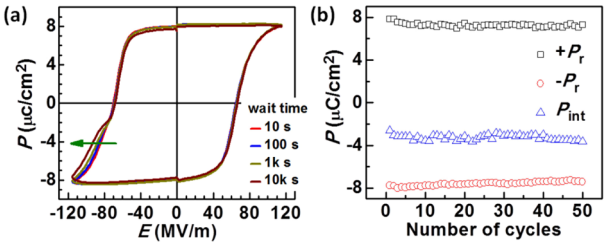

Figure 4. (a) Retention and (b) write/erase endurance of the intermediate polarization state.

intermediate state remains the same and its width increases with the retention time. For the endurance test, combinations of half and full electrical sequences were applied, and the data in Figure 4b show that no obvious degradation of the intermediate state was observed over 50 cycles.

The nature of space-charge injection and accumulation was elucidated by the leakage $I-V$ measurements of the devices. Unlike the inorganic counterparts, the transport mechanism in P(VDF−TrEE) polymer devices has not been thoroughly investigated so far. Figure 5 shows the leakage $I-V$ curves of P(VDF−TrEE) capacitors with organic layer thicknesses of 156 and 286 nm, respectively. In the past, several conducting mechanisms have been proposed for ferroelectric capacitors,[31−34] such as the bulk-limited Pool−Frenkel conduction in which the current is dominated by electrons hopping among defects,[31] the Schottky emission conduction for which the current is limited by the interface Schottky barrier,[32,35] and the space-charge-limited current (SCLC) conduction, where the current is limited by the space-charge layer formed at the

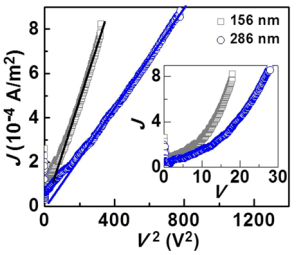

Figure 5. Typical leakage data for films with thicknesses of 156 nm (gray) and 286 nm (blue). The straight lines are fitting results according to SCLC model. Inset: J vs V curves in the linear scale.

electrode−film interface.[33,36] These models are featured with different equations, and fitting the $I-V$ data to these equations is commonly used to determine the conduction mechanism.

In our case, unreasonable values of the dielectric constant or depletion length are obtained when Pool−Frenkel and Schottky emission models are used for data fitting (Supporting Information, Figure S4). On the other hand, the $I-V$ data can be well fitted by using the SCLC model according to the following equation:

$$J = \frac{9}{8}\mu_{\text{eff}}\varepsilon_0\varepsilon_r\frac{V^2}{d^3} \quad (1)$$

where J, μ_{eff}, ε_0, ε_r, d, and V are the current density, effective carrier mobility, absolute dielectric constant, relative dielectric constant (∼10, as shown in Figure 2b), thickness of the P(VDF−TrEE) film, and applied voltage, respectively. The fitting, as shown in Figure 5, leads to $\mu_{\text{eff}} = 9.0 \times 10^{-17}$ and 2.7×10^{-16} m^2/V·s, respectively, for 156 and 286 nm P(VDF−TrEE) films. These values are much smaller than that reported for the PVDF polymer (∼10^{-10} m^2/V·s) by the method of radiation-induced conductivity using laser/X-ray as the radiation source.[37] Such a discrepancy has also been reported for other polymers such as polyethylene, which may be attributed to the different excitation conditions of the measurement methods.[38,39] Other factors such as the crystallization and doping level may also have some effect.[38] We also estimated the free carrier density n of P(VDF−TrEE) films through $n = \sigma/e\mu$, where σ is the conductivity and e is the electron charge. The values of n fall in the range of $(1-4) \times 10^{17}$/cm^3 for the two P(VDF−TrEE) films. This value is quite close to the density of states near the Fermi level of the PVDF polymer, taking into account the radius of the carrier wave function, which is on the order of 1 Å^{-1}.[40] This consistency underlines the validity of not only the above estimation of the carrier mobility but also the SCLC as the transport mechanism in the P(VDF−TrEE) devices. The good fitting to the SCLC model suggests that the injection and accumulation of electrons at the polymer−copper electrode interface are responsible for the substeps in the $P-E$ loops, as shown in Figure 3d.

To explain the subswitching behavior observed in the P(VDF−TrFE) capacitors, we propose the model shown in the schematic in Figure 6. It is known that an interface field (E_i) exists between the electrode and ferroelectric polymer due to the polarization-induced screening effect, which induces the dynamic injection and accumulation of charges (Q_t) into the polymer.[41] These charges are trapped by defects such as the grain boundaries or the crystalline/amorphous interfaces. They couple with the adjacent ferroelectric polarizations (P) and hinder their switching (Figure 6a). Figure 6b shows a typical half sequence (① to ③) applied on the devices followed by a full

dx.doi.org/10.1021/am5050136 | ACS Appl. Mater. Interfaces 2014, 6, 19057−19063

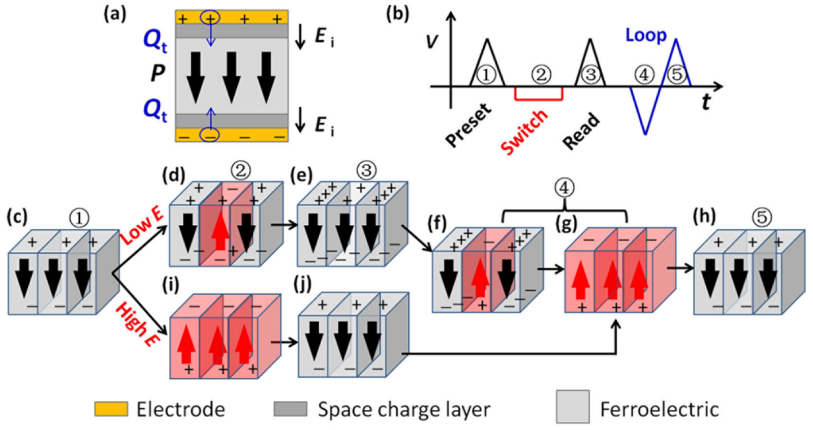

Figure 6. Schematic illustration of ferroelectric switching in a half sequence that produces anomalous switching loops in the PVDF devices. (a) At the interface between the electrode and film, electric field E_i drives partially screened charges into the polymer, and the trapped charges (Q_t) at the defect sites are coupled with the polarization (P). (b) Schematic of a half sequence (① to ③), followed by a subsequent P–E loop scan (④ and ⑤). (c–j) Corresponding domain and charge states schematically shown for the ferroelectric switching of both low- and high-switching electric field cases.

loop test (④ to ⑤). The characteristics of space charges and their coupling with polarization are dynamically modulated by the applied electric field in the half sequences (as shown in c to j). When the electric field is not high enough, only some of the domains are switched (c to h). An inhomogeneous distribution of the trapped charges could be formed during such a process (e), leading to the intermediate states in the P–E loops (f to g). On the other hand, these intermediate states are eliminated if the electric field in the half sequences is strong enough to unpin all of the domains from the coupling with the space charges (c to i to j), and no intermediate states exist in the subsequent P–E loops (Figure 6g). However, the situation is different in the full-sequence measurements: the magnitudes/polarities of electric pulses are well balanced so that the ferroelectric domains can switch "normally" without any substable states (Figure 3c).

It is insightful to compare the organic P(VDF–TrFE) with the inorganic ferroelectrics such as $BiFeO_3$ in terms of defects and switching characteristics. In $BiFeO_3$, the trapped charges mainly originate from the point defects such as oxygen vacancies, which are homogeneously distributed and coupled with the polarizations.[12,13,42] Such a coupling could be stabilized by thermal annealing, inducing stable substates in the ferroelectric switching loops. In addition, electron injection at the ferroelectric/metal electrode interface could also pin the domains and affect the shape of the P–E loops especially after prolonged cycling.[43] In the P(VDF–TrEE) polymers, however, neutral defects due to molecular conformation and packing are dominant.[22] Because the defects near the polymer/electrode interfaces are featured with shallow energy levels,[24,25] the trapped space charges could be easily released when the external reversed electric field is strong enough. This results in a weaker charge–polarization coupling compared to that for the inorganic counterparts. The overlapped positive branches of the P–E loops (Figure 3d) and the recovery of the P–E loops to the initial one after several scans of complete hysteresis loops (Supporting Information, Figure S5) further suggest that the trapped charge states in the P(VDF–TrEE) polymer can be easily emptied. We should note here that the bonding and structural nature of the PVDF–electrode interface remains as an open question; previous works suggest weaker interface chemical bonding and strain coupling in the organic devices compared to those for the inorganic counterparts.[44,45] In future studies, intentionally introducing new defects with deep energy levels through doping[46] and promoting the concentration of defect densities through high-energy irradiation[47] may be viable approaches to realizing stable multimemory states in P(VDF–TrEE) copolymers.

IV. CONCLUSION

In summary, we demonstrated that the ferroelectric P–E loops of P(VDF–TrEE) polymer capacitors could be electrically controlled and intermediate states with tailored polarizations were prepared by applying half sequences. We also found that the space-charge-limited current is the main leakage mechanism in such devices. Stable subswitching states were realized by leveraging the electrical coupling between the ferroelectric polarizations and space charges. Our experiment may open doors toward advancing high-density multilevel data storage devices based on organic ferroelectric materials.

■ ASSOCIATED CONTENT

Supporting Information

Data on the characterization and polarization switching behavior for the P(VDF-TrEE) copolymer films. This material is available free of charge via the Internet at http://pubs.acs.org.

■ AUTHOR INFORMATION

Corresponding Author

*E-mail: tao.wu@kaust.edu.sa.

Notes

The authors declare no competing financial interest.

■ ACKNOWLEDGMENTS

This work is supported by KAUST.

■ REFERENCES

(1) Scott, J. F.; Araujo, C. A. Ferroelectric Memories. *Science* **1989**, *246*, 1400–1405.

(2) Ahn, C. H.; Tybell, T.; Antognazza, L.; Char, K.; Hammond, R. H.; Beasley, M. R.; Fischer, O.; Triscone, J. M. Local, Nonvolatile Electronic Writing of Epitaxial $Pb(Zr_{0.52}Ti_{0.48})O_3/SrRuO_3$ Heterostructures. *Science* **1997**, *276*, 1100–1103.

(3) Scott, J. F. Applications of Modern Ferroelectrics. *Science* **2007**, *315*, 954−959.
(4) Yuan, Y. B.; Reece, T. J.; Sharma, P.; Poddar, S.; Ducharme, S.; Gruverman, A.; Yang, Y.; Huang, J. S. Efficiency Enhancement in Organic Solar Cells with Ferroelectric Polymers. *Nat. Mater.* **2011**, *10*, 296−302.
(5) Lu, H.; Bark, C. W.; Esque de los Ojos, D.; Alcala, J.; Eom, C. B.; Catalan, G.; Gruverman, A. Mechanical Writing of Ferroelectric Polarization. *Science* **2012**, *336*, 59−61.
(6) Fong, D. D.; Stephenson, G. B.; Streiffer, S. K.; Eastman, J. A.; Auciello, O.; Fuoss, P. H.; Thompson, C. Ferroelectricity in Ultrathin Perovskite Films. *Science* **2004**, *304*, 1650−1653.
(7) Lichtensteiger, C.; Triscone, J. M. Ferroelectricity and Tetragonality in Ultrathin $PbTiO_3$ Films. *Phys. Rev. Lett.* **2005**, *94*, 047603.
(8) Stengel, M.; Vanderbilt, D.; Spaldin, N. A. Enhancement of Ferroelectricity at Metal−Oxide Interfaces. *Nat. Mater.* **2009**, *8*, 392−397.
(9) Tsymbal, E. Y.; Kohlstedt, H. Tunneling Across a Ferroelectric. *Science* **2006**, *313*, 181−183.
(10) Gajek, M.; Bibes, M.; Fusil, S.; Bouzehouane, K.; Fontcuberta, J.; Barthélémy, A.; Fert, A. Tunnel Junctions with Multiferroic Barriers. *Nat. Mater.* **2007**, *6*, 296−302.
(11) Park, M. H.; Lee, H. J.; Kim, G. H.; Kim, Y. J.; Kim, J. H.; Lee, J. H.; Hwang, C. S. Tristate Memory Using Ferroelectric−Insulator−Semiconductor Heterojunctions for 50% Increased Data Storage. *Adv. Funct. Mater.* **2011**, *21*, 4305.
(12) Folkman, C. M.; Baek, S. H.; Nelson, C. T.; Jang, H. W.; Tybell, T.; Pan, X. Q.; Eom, C. B. Study of Defect-Dipoles in an Epitaxial Ferroelectric Thin Film. *Appl. Phys. Lett.* **2010**, *96*, 052903.
(13) Lee, D.; Jeon, B. C.; Baek, S. H.; Yang, S. M.; Shin, Y. J.; Kim, T. H.; Kim, Y. S.; Yoon, J. G.; Eom, C. B.; Noh, T. W. Active Control of Ferroelectric Switching Using Defect-Dipole Engineering. *Adv. Mater.* **2012**, *24*, 6490.
(14) Auciello, O.; Scott, J. F.; Ramesh, R. The Physics of Ferroelectric Memories. *Phys. Today* **1998**, *7*, 22−27.
(15) Horiuchi, S.; Tokura, Y. Organic Ferroelectrics. *Nat. Mater.* **2008**, *7*, 357−366.
(16) Naber, R. C. G.; Asadi, K.; Blom, P. W. M.; de Leeuw, D. M.; de Boer, B. Organic Nonvolatile Memory Devices Based on Ferroelectricity. *Adv. Mater.* **2010**, *22*, 933−945.
(17) Liang, S.; Kang, Y.; Tiraferri, A.; Giannelis, E. P.; Huang, X.; Elimelech, M. Highly Hydrophilic Polyvinylidene Fluoride (PVDF) Ultrafiltration Membranes via Postfabrication Grafting of Surface-tailored Silica Nanoparticles. *ACS Appl. Mater. Interfaces* **2013**, *5*, 6694−6703.
(18) Liu, S. H.; Zhai, J. W.; Wang, J. W.; Xue, S. X.; Zhang, W. Q. Enhanced Energy Storage Density in Poly(Vinylidene Fluoride) Nanocomposites by a Small Loading of Suface-hydroxylated $Ba_{0.6}Sr_{0.4}TiO_3$ Nanofibers. *ACS Appl. Mater. Interfaces* **2014**, *6*, 1533−1540.
(19) Khan, M. A.; Bhansali, U. S.; Zhang, X. X.; Saleh, M. M.; Odeh, I.; Alshareef, H. N. Doped Polymer Electrodes for High Performance Ferroelectric Capacitors on Plastic Substrates. *Appl. Phys. Lett.* **2012**, *101*, 143303.
(20) Yang, S. M.; Yoon, J. G.; Noh, T. W. Nanoscale Studies of Defect-mediated Polarization Switching Dynamics in Ferroelectric Thin Film Capacitors. *Curr. Appl. Phys.* **2011**, *11*, 1111−1125.
(21) Sharma, P.; Reece, T. J.; Ducharme, S.; Gruverman, A. High-resolution Studies of Domain Switching Behavior in Nano-structured Ferroelectric Polymers. *Nano Lett.* **2011**, *11*, 1970−1975.
(22) Sharma, P.; Nakajima, T.; Okamura, S.; Gruverman, A. Effect of Disorder Potential on Domain Switching Behavior in Polymer Ferroelectric Films. *Nanotechnology* **2013**, *24*, 015706.
(23) Hu, W. J.; Juo, D. M.; You, L.; Wang, J. L.; Chen, Y. C.; Chu, Y. H.; Wu, T. Universal Ferroelectric Switching Dynamics of Vinylidene Fluoride−trifluoroethylene Copolymer Films. *Sci. Rep.* **2014**, *4*, 4772.
(24) Lew, C.; Thompson, M. O. Characterizing Trapped Charge Dynamics in Imprinted Poly(Vinylidene Fluoride−trifluoroethylene) Ferroelectric Thin Films Using the Fast Ramp Thermally Stimulated Current Technique. *J. Appl. Phys.* **2009**, *105*, 054112.
(25) Lew, C.; Thompson, M. O. Quantifying Electronic Charge Trap States and the Effect of Imprint on Ferroelectric Poly(Vinylidene Fluoride−trifluoroethylene) Thin Films. *J. Appl. Phys.* **2010**, *107*, 104110.
(26) Scott, J. F. *Ferroelectric Memories*; Springer: Berlin, 2000; Chapter 6.
(27) Li, J.; Taguchi, D.; Yang, W. O.; Manaka, T.; Iwamoto, M. Interaction of Interfacial Charge and Ferroelectric Polarization in a Pentacene/Poly(Vinylidene Fluoride−Trifluoroethylene) Double-Layer Device. *Appl. Phys. Lett.* **2011**, *99*, 063302.
(28) Kam, B.; Li, X. R.; Cristoferi, C.; Smits, E. C. P.; Mityashin, A.; Schols, S.; Genoe, J.; Gelinck, G.; Heremans, P. Origin of Multiple Memory States in Organic Ferroelectric Field-Effect Transistors. *Appl. Phys. Lett.* **2012**, *101*, 033304.
(29) Tripathi, A. K.; van Breemen, A. J. J. M.; Shen, J.; Gao, Q.; Ivan, M. G.; Reimann, K.; Meinders, E. R.; Gelinck, G. H. Multilevel Information Storage in Ferroelectric Polymer Memories. *Adv. Mater.* **2011**, *23*, 4146.
(30) Hwang, S. K.; Bae, I.; Kim, R. H.; Park, C. Flexible Non-Volatile Ferroelectric Polymer Memory with Gate-Controlled Multilevel Operation. *Adv. Mater.* **2012**, *24*, 5910−5914.
(31) Frenkel, J. On Pre-breakdown Phenomena in Insulators and Electronic Semi-conductors. *Phys. Rev.* **1938**, *54*, 647−648.
(32) Stolichnov, I.; Tagantsev, A. Space-charge Influenced-injection Model for Conduction in $Pb(Zr_xTi_{1-x})O_3$ Thin Films. *J. Appl. Phys.* **1998**, *84*, 3216−3225.
(33) Rose, A. Space-charge-limited Currents in Solids. *Phys. Rev.* **1955**, *97*, 1538−1544.
(34) Pintilie, L.; Vrejoiu, I.; Hesse, D.; LeRhun, G.; Alexe, M. Ferroelectric Polarization−leakage Current Relation in High Quality Epitaxial $Pb(Zr,Ti)O_3$ Films. *Phys. Rev. B* **2007**, *75*, 104103.
(35) Bera, A.; Peng, H. Y.; Lourembam, J.; Shen, Y. D.; Sun, X. W.; Wu, T. A Versatile Light-switchable Nanorod Memory: Wurtzite ZnO on Perovskite $SrTiO_3$. *Adv. Funct. Mater.* **2013**, *23*, 4977−4984.
(36) Cui, Y. M.; Peng, H. Y.; Wu, S. X.; Wang, R. M.; Wu, T. Complementary Charge Trapping and Ionic Migration in Resistive Switching of Rare-earth Manganite $TbMnO_3$. *ACS Appl. Mater. Interfaces* **2013**, *5*, 1213−1217.
(37) Hayashi, K.; Takemura, M.; Tsubakihara, H.; Kubo, U. Carrier Mobility in Vinylidene Fluoride−trifluoroethylene Copolymer. *Jpn. J. Appl. Phys.* **1995**, *34*, 212−213.
(38) Martin, E. H.; Hirsch, J. Electron Induced Conduction in Plastics. I. Determination of Carrier Mobility. *J. Appl. Phys.* **1972**, *43*, 1001−1007.
(39) Wintle, H. J. Decay of Static Electrification by Conduction Processes in Polyethylene. *J. Appl. Phys.* **1970**, *41*, 4004−4007.
(40) Singh, R.; Sinha, R. D. P.; Kaur, A.; Kumar, J. AC Conductivity and Dielectric Relaxation Behavior of Solution Grown Poly(Vinylidene Fluoride) Films. *Ferroelectrics* **2005**, *329*, 91−99.
(41) Grossmann, M.; Lohse, O.; Bolten, D.; Boettger, U.; Schneller, T.; Waser, R. The Interface Screening Model as Origin of Imprint in $PbZr_xTi_{1-x}O_3$ Thin Films. I. Dopant, Illumination, and Bias Dependence. *J. Appl. Phys.* **2002**, *92*, 2680−2687.
(42) You, L.; Chua, N. T.; Yao, K.; Chen, L.; Wang, J. L. Influence of Oxygen Pressure on the Ferroelectric Properties of Epitaxial $BiFeO_3$ Thin Films by Pulsed Laser Deposition. *Phys. Rev. B* **2009**, *80*, 024105.
(43) Zou, X.; You, L.; Chen, W. G.; Ding, H.; Wu, D.; Wu, T.; Chen, L.; Wang, J. L. Mechanism of Polarization Fatigue in $BiFeO_3$. *ACS Nano* **2012**, *6*, 8997−9004.
(44) Lukashev, P. V.; Paudel, T. R.; López-Encarnación, J. M.; Adenwalla, S.; Tsymbal, E. Y.; Velev, J. P. Ferroelectric Control of Magnetocrystalline Anisotropy at Cobalt/Poly(Vinylidene Fluoride) Interfaces. *ACS Nano* **2012**, *6*, 9745−9750.
(45) Zhao, D.; Katsouras, I.; Li, M. Y.; Asadi, K.; Tsurumi, J.; Glasser, G.; Takeya, J.; Blom, P. W. M.; de Leeuw, D. M. Polarization Fatigue of Organic Ferroelectric Capacitors. *Sci. Rep.* **2014**, *4*, 5075.

(46) Nakhmanson, S. M.; Nardelli, M. B.; Bernholc, J. Ab Initio Studies of Polarization and Piezoelectricity in Vinylidene Fluoride and BN-based Polymers. *Phys. Rev. Lett.* **2004**, *92*, 115504.
(47) Zhang, Q. M.; Bharti, V.; Zhao, X. Giant Electrostriction and Relaxor Ferroelectric Behavior in Electron-irradiated Poly(Vinylidene Fluoride−Trifluoroethylene) Copolymer. *Science* **1998**, *280*, 2101−2104.